Received: 20 September 2018 | Revised: 5 December 2018 | Accepted: 21 December 2018

DOI: 10.1002/mrm.27660

FULL PAPER

Magnetic Resonance in Medicine

Dependence of the MR signal on the magnetic susceptibility of blood studied with models based on real microvascular networks

Xiaojun Cheng[1,2] | Avery J.L. Berman[2] | Jonathan R. Polimeni[2,3] | Richard B. Buxton[4] | Louis Gagnon[2,5] | Anna Devor[2,4,6] | Sava Sakadžić[2] | David A. Boas[1,2]

[1]Neurophotonics Center, Department of Biomedical Engineering, Boston University, Massachusetts

[2]Athinoula A. Martinos Center for Biomedical Imaging, Department of Radiology, Massachusetts General Hospital, Harvard Medical School, Charlestown, Massachusetts

[3]Division of Health Sciences and Technology, Massachusetts Institute of Technology, Cambridge, Massachusetts

[4]Department of Radiology, University of California, San Diego, La Jolla, California

[5]Department of Radiology and Nuclear Medicine, Faculty of Medicine, Laval University, Quebec, Canada

[6]Department of Neurosciences, University of California, San Diego, La Jolla, California

Correspondence
Xiaojun Cheng, Neurophotonics Center, Department of Biomedical Engineering, Boston University, Boston, MA 02215.
Email: xcheng17@bu.edu

Funding information
National Institutes of Health (NIH)/National Institute of Biomedical Imaging and Bioengineering (grants P41-EB015896 and R01-EB019437); NIH/National Institute of Neurological Disorders and Stroke (grant R01-NS036722); the BRAIN Initiative (NIH NIMH grants R01-MH111419 and R01-MH111359); and the MGH/HST Athinoula A. Martinos Center for Biomedical Imaging.

Purpose: The primary goal of this study was to estimate the value of β, the exponent in the power law relating changes of the transverse relaxation rate and intra-extravascular local magnetic susceptibility differences as $\Delta R_2^* \propto (\Delta\chi)^\beta$. The secondary objective was to evaluate any differences that might exist in the value of β obtained using a deoxyhemoglobin-weighted $\Delta\chi$ distribution versus a constant $\Delta\chi$ distribution assumed in earlier computations. The third objective was to estimate the value of β that is relevant for methods based on susceptibility contrast agents with a concentration of $\Delta\chi$ higher than that used for BOLD fMRI calculations.

Methods: Our recently developed model of real microvascular anatomical networks is used to extend the original simplified Monte-Carlo simulations to compute β from the first principles.

Results: Our results show that $\beta = 1$ for most BOLD fMRI measurements of real vascular networks, as opposed to earlier predictions of $\beta = 1.5$ using uniform $\Delta\chi$ distributions. For perfusion or fMRI methods based on contrast agents, which generate larger values for $\Delta\chi$, $\beta = 1$ for $B_0 \leq 9.4$ T, whereas at 14 T β can drop below 1 and the variation across subjects is large, indicating that a lower concentration of contrast agent with a lower value of $\Delta\chi$ is desired for experiments at high B_0.

Conclusion: These results improve our understanding of the relationship between R_2^* and the underlying microvascular properties. The findings will help to infer the cerebral metabolic rate of oxygen and cerebral blood volume from BOLD and perfusion MRI, respectively.

KEYWORDS
BOLD fMRI, contrast agents, microvascular network, modeling, perfusion MRI

1 | INTRODUCTION

The transverse relaxation rate, R_2^*, of the MR signal is related to the dephasing rate of protons within an imaging voxel, which is sensitive to magnetic susceptibility–induced changes in the local magnetic field, ΔB. One way to alter the magnetic susceptibility is to use exogenous agents such as gadolinium-based contrast agents, delivered as a bolus injection as in the dynamic susceptibility contrast technique, or blood-pool contrast agents such as ultrasmall superparamagnetic iron-oxide agents that have long plasma half-lives.[1-4] The increase of the transverse relaxation rate, ΔR_2^*, in response to contrast agent injection is a measure of cerebral blood volume (CBV), as $\Delta R_2^* \propto CBV \cdot \Delta\chi^{\beta}$,[5] in which $\Delta\chi$ is the magnetic susceptibility difference between blood and tissue and β is a parameter in the power law model of the susceptibility effect. In many cases, β is assumed to be 1 and the relation is simplified as $\Delta R_2^* \propto CBV \cdot \Delta\chi$.

Deoxyhemoglobin is another agent that can alter local magnetic susceptibility, because it is paramagnetic and its presence decreases the MR signal.[6,7] This endogenous agent provides a link between the MR signal and neuronal activity.[8-11] The BOLD signal is a complicated function of several underlying physiological variables including cerebral blood flow (CBF), cerebral metabolic rate of oxygen ($CMRO_2$), and CBV. The Davis model of calibrated fMRI describes the BOLD signal change during activation as $\delta BOLD = M(1 - rCMRO_2^{\beta} \bullet rCBF^{\alpha-\beta})$, where rCBF and $rCMRO_2$ are the relative changes in CBF and $CMRO_2$ normalized by their baseline values.[12] Here, M is a normalization factor that can be obtained from hypercapnia or hyperoxia calibration techniques, and α is the exponent in the flow-volume relation $rCBV = rCBF^{\alpha}$.[12-15] The parameter β in the original Davis model has the same physiological meaning as in the susceptibility effect (i.e., $\Delta R_2^* \propto \Delta\chi^{\beta}$). With these parameters identified, the Davis model provides a method to obtain $rCMRO_2$ during neuronal activation from a combination of BOLD measurements and CBF measurements, with the latter typically acquired using arterial spin labeling.[16,17]

The value of the parameter β was originally estimated using Monte-Carlo simulations of proton diffusion through random distributions of infinite cylinders, and the resulting value was found to be 1.5 at $B_0 = 1.5$ T.[5] The main source that gives rise to a nonlinear susceptibility effect, $\beta \neq 1$, is extravascular proton diffusion. For large vessels such as veins, proton diffusion can be ignored and the static dephasing calculations give $\beta = 1$, whereas for small vessels where diffusion is prominent, $\beta = 2$.[11,18,19] The motional narrowing effect of diffusion around small vessels leads to the same amount of deoxyhemoglobin, having a weaker effect on the BOLD signal compared with larger veins.[20] In addition, the cylinders models[5] are simplified versions of a real vascular network in which the more complicated structures, such as vessel curvature and bifurcations, found in anatomical vascular networks, are not considered and the size distribution of vessels are not necessarily modeled. More importantly, unlike exogenous contrast agents, the concentration of deoxyhemoglobin is not uniform throughout the vascular network, and instead there is a gradient of deoxyhemoglobin concentration from the arterial side to the venous side of the vascular network. Thus, the value of β, particularly in the Davis model for fMRI, needs a more comprehensive investigation.

In vivo experiments in humans have found that $\beta = 1$ in calibrated BOLD experiments at 1.5 T, 3 T, and 7 T,[21] which is consistent with recent multicompartment vascular modeling studies that suggest $\beta = 1$ at 3 T.[22,23] These vascular modeling studies estimated β and α indirectly by treating them as free parameters of the Davis model in simulations of the BOLD signals. However, these studies have abandoned the physiological meanings of the parameters and did not explicitly determine β through relating ΔR_2^* directly to $\Delta\chi$. In the present study, we obtain the value of β from first principles by performing calculations using real microvascular networks, obtained using in vivo 2-photon measurements in the cerebral cortex of mice, for both deoxyhemoglobin-weighted and uniform $\Delta\chi$ distributions, with the concentration range relevant for BOLD fMRI. We find that the value of β decreases with magnetic field strength B_0. At lower field strengths, β depends on the details of the vasculature and can vary across subjects and regions for a uniform distribution of $\Delta\chi$. However, $\beta = 1$ for most BOLD fMRI measurements at $B_0 \geq 3$ T, where $\Delta\chi$ is weighted by deoxyhemoglobin concentration, which is a more realistic assumption for the BOLD signals. Setting $\beta = 1$ greatly simplifies macroscopic models such as the Davis model.[12] In addition, the value of β has also been computed with a uniform distribution of $\Delta\chi$ at a higher concentration relevant for perfusion or functional imaging based on contrast agents. For imaging based on contrast agents, $\beta = 1$ for $B_0 \leq 9.4$ T, whereas at 14 T β drops below 1 and the variation across subjects is large, which indicates that a lower concentration of $\Delta\chi$ is desired for experiments at high B_0.

2 | METHODS

2.1 | Microvascular network and vascular anatomical network modeling

The microvascular networks used here were obtained using in vivo 2-photon imaging of the cerebral cortex of C57BL/6 mice and published in previous studies.[23,24] We used 6 unique microvascular networks obtained from 6 different mice. The vascular anatomical network (VAN) model was then applied to these vascular networks. The VAN model is a bottom-up model that computes blood flow and oxygenation distributions within microscopic vasculature and the resulting MR signal.[23,24] The steady-state

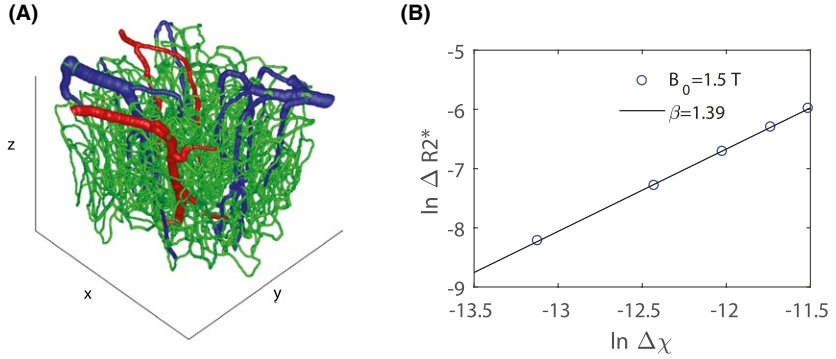

FIGURE 1 A, Example of a graphed vascular network obtained from 2-photon microscopy measurements (blue, veins; red, arteries; green, capillaries). B, ln ΔR_2^* as a function of ln $\Delta\chi$ for the vascular network in (A) at $B_0 = 1.5$T. The value of β is obtained from the slope of the linear fit, which is 1.39 in this example. Here, $\Delta\chi$ distribution is uniform within the BOLD range of 2×10^{-7} to 12×10^{-7}

oxygen distribution is obtained by solving the advection-diffusion equation until it reaches equilibrium.[25,26] After the deoxyhemoglobin distribution is computed from the oxygen distribution, the MR signal $S(t)$ can be obtained from Monte-Carlo simulations of proton diffusion through inhomogeneous magnetic fields. A comparison with the cylinder model and more information about the oxygen distribution are shown in Supporting Information Figures S1 and S2.

The magnetic field experienced by a proton is the sum of the magnetic field perturbations produced by all of the vessels in the VAN, each with a magnetic susceptibility $\Delta\chi$. We model BOLD, in which $\Delta\chi$ is given by the deoxyhemoglobin content of each vessel, compared with a constant $\Delta\chi$ distrubution across vessels. The magnetic field inhomogeneity $\Delta B(\vec{x})$ is computed by convolving $\Delta\chi$ with the magnetic field induced by a unit cube $\Delta B_{cube} = \frac{\left(\frac{a}{r}\right)a^3}{r^3}\left(3cos^2\theta - 1\right)B_0$, in which a is the grid size (1 μm) and r and θ are polar coordinates. The phase accumulation of the Nth proton is $\Delta\phi_n(t) = \gamma \Delta B_n(t)\,\Delta t$, with $\gamma = 2.675 \times 10^5$ rad/T/ms $= 2.675 \times 10^8$ rad/T/s being the gyromagnetic ratio and $\Delta B_n(t)$ being the local magnetic field perturbation experienced by the Nth proton at time t. The initial positions of 1×10^7 protons within the VAN voxel are random and drawn from a uniform distribution. The diffusion coefficient of protons is set to be 1×10^{-5} cm^2/s $= 1 \times 10^{-9}$ m^2/s,[23,27] and protons are not allowed to diffuse across the vessel wall. The time step for Monte-Carlo simulations is dt $= 0.2$ ms $= 2 \times 10^{-4}$ seconds and the TE $= 30$ ms $= 3 \times 10^{-2}$ seconds. A smaller time step of $dt = 0.01$ ms is used for large $B_0 \geq 9.4$T and $\Delta\chi$ $1 - 10 \times 10^6$, as explained in Supporting Information Figure S3. The MR signal at each time step is $S(t) = Re\{\frac{1}{N}\sum_{n=1}^{N} e^{\phi_n(t)}\}$, where the intravascular contribution is $\phi_{n,intra}(t) = \sum_{k=1}^{t/dt} -T^*_{2,vessel}(x(k))$ and the extravascular contribution is $\phi_{n,intra}(t) = \sum_{k=1}^{t/dt} i\Delta\phi_n(t) - T_{2,tissue}(x(k))$. The values of the intrinsic $T^*_{2,vessel}$ and $T_{2,tissue}$ depend on field strength and blood oxygenation and are obtained experimentally.[28] (A more detailed explanation of the simulations is found in Refs 23 and 24.) In the present study, we simulate only the baseline state and gradient-echo signals to study the susceptibility effect on the reversible transverse relaxation rate R_2^*. Spin-echo signals and changes driven by functional activation, including dynamic vessel dilations and metabolic rate variations, can also be modeled if needed using the same framework, which are not examined in this study.[23]

2.2 | Transverse relaxation rate and its relation to magnetic susceptibility change

For gradient-echo imaging, the MR signal at TE is approximated as

$$S(TE) = \exp(-R_2^* \cdot TE). \tag{1}$$

The transverse relaxation rate R_2^* is obtained through

$$R_2^* = -\ln(S(TE))/TE. \tag{2}$$

Because $\Delta R_2^* \propto (\Delta\chi)^\beta$,

$$\ln \Delta R_2^* = \beta \ln \Delta\chi + \text{constant}. \tag{3}$$

We obtain β from fitting the ln ΔR_2^* versus ln $\Delta\chi$ curve with varying $\Delta\chi$. To obtain β that is relevant for BOLD MRI, we compute R_2^* for gradient-echo signals in 2 different ways. The first uses a constant $\Delta\chi$ across all vessels, with a value ranging from 2×10^{-7} to 12×10^{-7}, which is of the same order as the $\Delta\chi$ concentration induced by deoxyhemoglobin in BOLD measurement and is referred to as the "uniform $\Delta\chi$ distribution." This is similar to how β has been computed previously using infinite cylinders.[5,29] In the second method, to account for the influence of the nonuniform deoxyhemoglobin concentration across the vascular tree on the BOLD signal, the magnetic susceptibility inside vessels is weighted microscopically as

$$\Delta\chi(\vec{r}) = \Delta\chi Hct(1 - SO_2(\vec{r})), \tag{4}$$

where SO_2 is the oxygen saturation obtained from the oxygen advection diffusion modeling and Hct is the hematocrit,

which is assumed to be 0.3 in capillaries and 0.4 in arteries and veins.[22] This β calculation is referred to as the "deoxyhemoglobin-weighted $\Delta\chi$ distribution." In this case, $\Delta\chi$ is modulated from 2×10^{-6} to 4×10^{-6}, and β is similarly obtained from the slope of the $\ln\Delta R_2^*$ versus $\Delta\chi$ curve. For reference, $\Delta\chi$ is typically $4\pi\bullet\ 0.264\times10^{-6} = 3.32\times10^{-6}$, which is the susceptibility difference between fully oxygenated and fully deoxygenated red blood cells.[30] An example of ΔR_2^* versus $\Delta\chi$ for the uniform $\Delta\chi$ distribution at 1.5 T for 1 vascular network (Figure 1A) is shown in Figure 1B. Unless stated otherwise, TE = 30 ms is used to fix the length of proton diffusion during the simulated MR experiment. We did not explore the nonexponential decay of $S(t)$ at early times in the current study, and we term R_2^* as the apparent transverse relaxation rate,[30] the attenuation of the signal at TE relative to that at TE = 0. If not stated otherwise, the orientation of the static magnetic field B_0 is in the z-direction, perpendicular to the surface of the cerebral cortex.

One final $\Delta\chi$ range is used to examine the influence of contrast agents on β. A higher concentration of $\Delta\chi$ ranging from 1×10^{-6} to 10×10^{-6} corresponding to vascular gadolinium-diethylenetriaminepentacetate concentrations of 3.6 mM to 36 mM,[5] which covers most of the $\Delta\chi$ range for contrast-enhanced perfusion imaging and is referred to as the "contrast agent range," is also used to compute β, in which $\Delta\chi$ was again set to a constant value across all vessels. This computation is referred to as the "contrast-enhanced $\Delta\chi$ distribution."

2.3 | Monte-Carlo simulations with the random cylinders model

To explore the effect of different size vessels on β at different field strengths B_0, we performed Monte-Carlo simulations of proton diffusion within and around randomly distributed magnetic cylinders—similar to the original simulations by Boxerman et al,[5] but with the size of the cylinders fixed in 1 configuration instead of using a distribution of sizes. The static magnetic field is $B_0\hat{z}$. The magnetic field at a point (x, y, z) in space induced by a single, infinitely long cylinder is[31]

$$\Delta B(x,y,z)/B_0 = \begin{cases} \frac{1}{2}\Delta\chi(R/r)^2\cos2\varphi\sin^2\theta, & r\geq R \\ \left(\frac{1}{6}\right)\Delta\chi\left(3\cos^2\theta-1\right), & r<R. \end{cases} \quad (5)$$

Here, θ is the angle between the cylinder and $\hat{z}$, r is the distance of a spatial point from the cylinder axis, and φ is the angle between projections in a plane orthogonal to the cylinder axis of $B_0\hat{z}$ and a line connecting the point and the cylinder axis. The radius of cylinders R is fixed for a single simulation, whereas the positions and orientations of the cylinders are random. A new configuration is generated for each cylinder size R from 1 μm to 5 μm = (1–5) $\times10^{-6}$ m, and each considered 5 different B_0 to obtain the size dependence of β at different field strengths. These cylinders and protons are contained in a box of size $L = 600\,\mu m = 6\times10^{-4}$ m in x, y, and z dimensions to match the dimensions of the simulated voxel used in the VAN simulations. We continue to add cylinders to the box until $N\pi R^2L/L^3$ is larger than 2%, where N is the total number of cylinders. We have also computed the results for $\frac{N\pi R^2L}{L^3} > 4\%$, to see the effect of cylinder densities. Distribution of $\Delta\chi$ is uniform with the contrast agent range from 1×10^{-6} to 10×10^{-6}. The BOLD range of $\Delta\chi$ from 2×10^{-7} to 12×10^{-7} is also used as a comparison. Proton diffusion was simulated to derive the MR signal following the same procedure as described previously for the VAN modeling. The values of R_2^* and β are obtained from Equations 2 and 3, respectively. SI units are used throughout this report.

3 | RESULTS

Results of the BOLD-relevant β obtained from our 6 unique VANs for both uniform $\Delta\chi$ distribution, which was used in earlier simulations with random cylinder models,[5] and deoxyhemoglobin-weighted $\Delta\chi$ distribution are shown in Figure 2A, B, respectively.

We see that the value of β is generally between 1 and 2, because a real vascular network is a mixture of large-producing ($\beta = 1$) and small-producing ($\beta = 2$) vessels. We also see that β can vary between the different vascular networks—likely because of differences in the size distribution of the vessels. The value of β obtained from the deoxyhemoglobin-weighted distribution is closer to the large-vessel size limit of $\beta = 1$, as in this case the venules that are larger in size maintain higher deoxyhemoglobin concentrations, and thus exert more influence on the diffusing protons than the generally smaller arterioles and capillaries. In both cases, β decreases with increasing B_0, which shows that the diffusion effect on β around small vessels is less important at higher fields. This indicates that β is expected to be more uniform across subjects and regions at higher magnetic field strengths.

The effect of the orientation of B_0 relative to the cortical surface normal axis on BOLD signals has been shown to have up to a 40% effect on BOLD signal amplitude.[24] This effect is due to the fact that the orientations of the vessels are not random and the spatial distribution is not uniform.[32] Here we investigate whether the orientation of B_0 has an effect on the value of β. Figure 3A,B shows the average β from the 6 VANs for B_0 transverse and is perpendicular to the surface of the cerebral cortex with both uniform and deoxyhemoglobin-weighted $\Delta\chi$ distribution. The difference between β obtained at the 2 orientations is less than 5% at 1.5 T and decreases with increasing B_0, which shows that the susceptibility effect

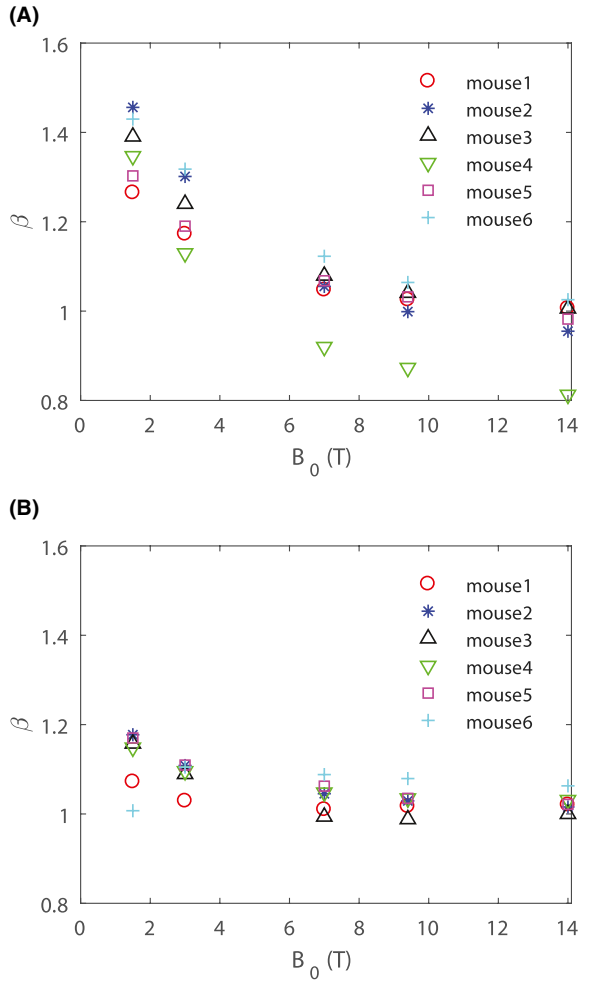

FIGURE 2 Value of β obtained from vascular anatomical network (VAN) modeling for uniform $\Delta\chi$ distribution (A) and deoxyhemoglobin-weighted $\Delta\chi$ distribution (B). B_0 is perpendicular to the surface of the cortex

depends less on the B_0orientation at higher fields. This further suggests a more spatially uniform β map at higher magnetic field strengths.

In all of these results, we have fixed the value of TE = 30 ms to fix the proton diffusion length. In practice, TE is chosen to match tissue T_2^*, which varies with B_0. The question arises as to whether the value of β changes with TE. In the ideal case, in which $S(t)$ decays truly exponentially, the apparent R_2^* obtained from $lnS(TE)/TE$ and β will not change. Figure 4 shows the mean value of β obtained from our 6 VANs for TE = 15 ms and 30 ms with uniform and deoxyhemoglobin-weighted $\Delta\chi$ distribution. The values of β are slightly different for different TEs due to the nonexponential decay of $S(t)$ at small t,[30] exhibiting a small increase for shorter TE with uniform $\Delta\chi$ distribution and negligible dependence on TE for deoxyhemoglobin-weighted $\Delta\chi$ distribution.

For perfusion or functional imaging based on intravascular contrast agents, the concentration of $\Delta\chi$ can be an order of magnitude higher than the range relevant for BOLD fMRI. Because the induced magnetic field inhomogeneity is proportional to $\Delta\chi \cdot B_0$, increasing $\Delta\chi$ has a similar effect as increasing B_0, which acts to decrease β. The values for β computed for the contrast agent range of $\Delta\chi$ from 1×10^{-6} to 10×6^{-6} with a uniform distribution is shown in Figure 5A. We see that $\beta \approx 1$ for $B_0 \leq 9.4$ T, which is smaller than the values computed in Figure 2A with the BOLD fMRI range of $\Delta\chi$, as expected. However, for $B_0 = 14$T, β drops below 1 and the variations across subjects is large. This indicates that at 14 T, a few large vessels dominate and the value of β is no longer between the theoretical predictions of 1 and 2 made under the assumption of a random distribution of vessels. This indicates that at 14 T, a lower concentration of $\Delta\chi$ is desired. In Figure 5B, β obtained from a lower concentration of $\Delta\chi$ from 1×10^{-6} to 3×6^{-6}, which is relevant for many dynamic susceptibility contrast studies,[33] is shown, where $\beta \approx 1$ at all field strengths. The time step in the Monte-Carlo simulations for $B_0 = 9.4$ T and 14 T is 0.01 ms instead of 0.2 ms, as in other simulations.

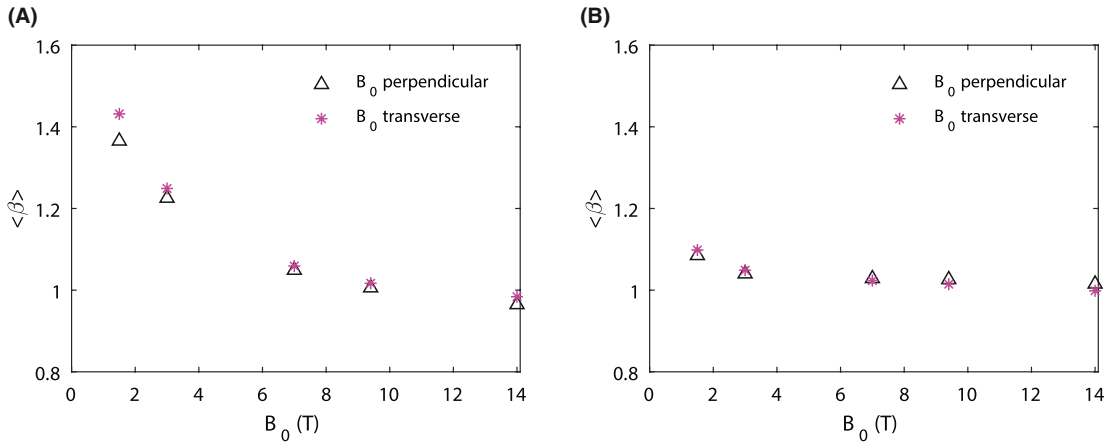

FIGURE 3 Mean value of β obtained from 6 VANs for B_0 transverse and perpendicular to the surface of the cerebral cortex with uniform $\Delta\chi$ distribution (A) and deoxyhemoglobin-weighted $\Delta\chi$ distribution (B)

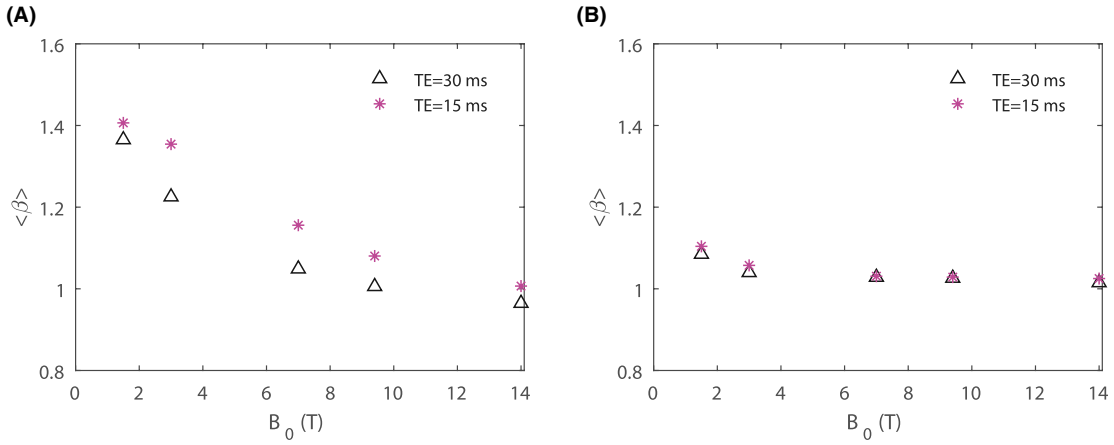

FIGURE 4 Mean value of β obtained from 6 VANs for TE = 15 ms and 30 ms with uniform $\Delta\chi$ distribution (A) and deoxyhemoglobin-weighted $\Delta\chi$ distribution (B)

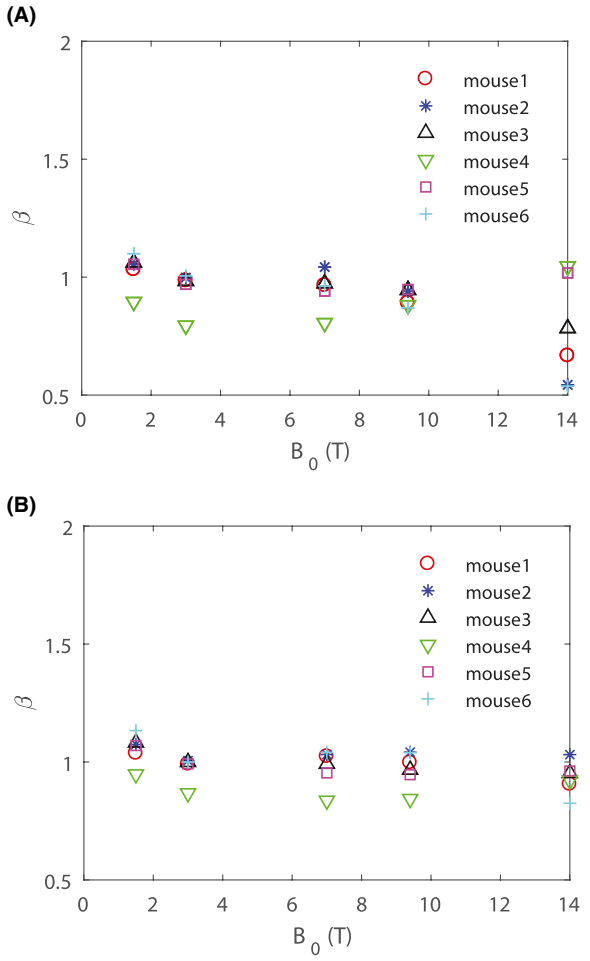

FIGURE 5 Value of β obtained from 6 VANs for uniform $\Delta\chi$ distribution within perfusion or functional imaging based on susceptibility contrast agents from 1×10^{-6} to 10×10^{-6} (A) and from 1×10^{-6} to 3×10^{-6} (B)

To help understand the behavior of β decreasing with increasing B_0, we explored the dependence of β on vessel radius and magnetic field strength B_0 with Monte-Carlo simulations using a random cylinder model, as described in the Materials and Methods section. The value of β is obtained for various radii R of randomly distributed cylinders at different magnetic field strengths, with each value calculated by averaging over 4 random cylinder configurations. Figure 6A, B shows the results of protons moving freely across vessel walls and no proton exchange across vessels walls, respectively. We see that vessel wall permeability has a negligible effect on β. The critical value of R, where β deviates from 1, is smaller at higher fields, indicating that the small vessels act more like large vessel at higher fields; thus, β is closer to the large vessel limit of $\beta = 1$. Figure 6C shows the results for a cylinder volume fraction of 4% (as opposed to 2% in the other simulations). These can be compared with simulations in the strict static dephasing regime, as shown in Figure 6D, where protons are not moving and the value of β is approximately 1, which further confirms that proton diffusion is the main cause of a nonlinear susceptibility effect ($\beta \neq 1$). For a typical capillary radius of 3μm, $\beta = 1$ for 7 T and above. This ensures that $\beta = 1$ for imaging regions consisting only of capillaries at 7 T and above for high-resolution fMRI. For a range of $\Delta\chi$ similar to that encountered in BOLD fMRI as shown in Figure 6E, β is significantly higher for capillaries, compared with the results obtained for a range of $\Delta\chi$, mimicking that found when using a contrast agent as in Figure 6A. Thus, assuming a uniform distribution of $\Delta\chi$ overestimates β for BOLD fMRI measurements, as the small capillaries with large β are weighted the same way as large veins.

4 | DISCUSSION

The parameter β, the exponent in a power law relationship between the change in transverse relaxation rate ΔR_2^* and changes in the magnetic susceptibility of blood $\Delta\chi$, is important in 2 physiological imaging contexts: (1) guiding

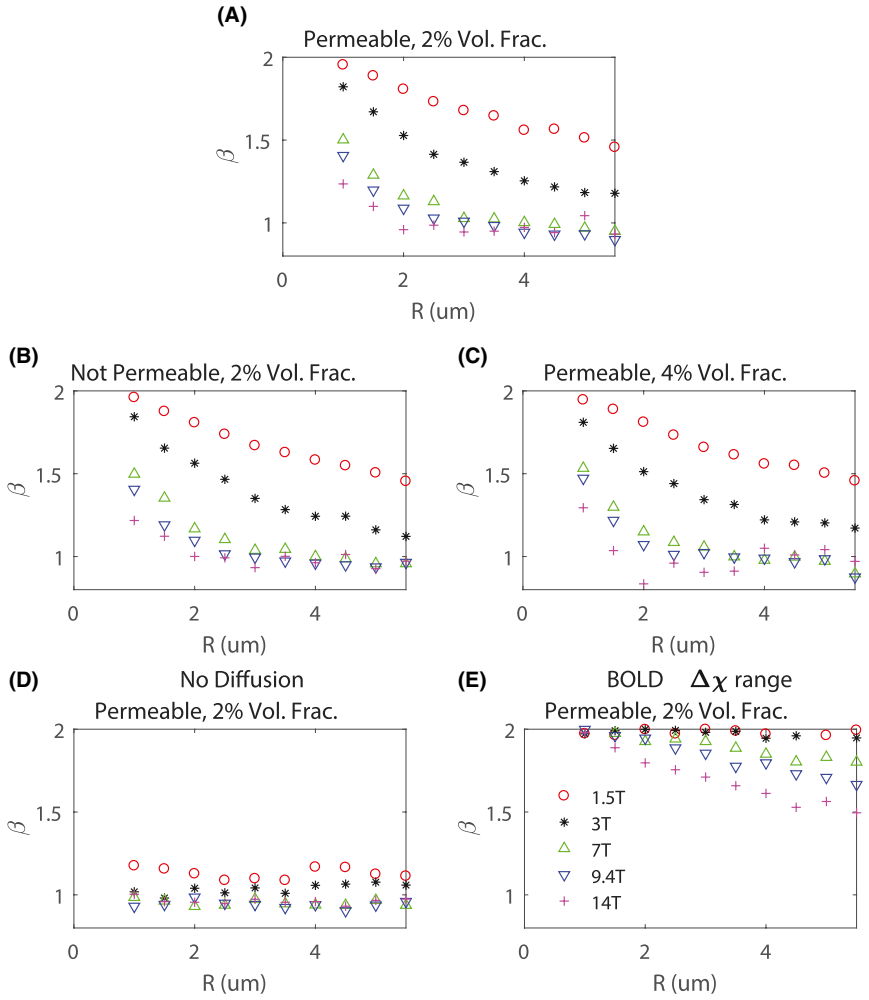

FIGURE 6 Susceptibility effect parameter β obtained for various vessel diameters corresponding to capillaries at different field strengths for Monte-Carlo simulations with freely diffusing protons (2% volume fraction) (A), for Monte-Carlo simulations with no proton exchange between intravasular and extravascular spaces (2% volume fraction) (B), for Monte-Carlo simulations with a cylinder volume fraction of 4% instead of 2% (C), for static dephasing with protons not moving (2% volume fraction) (D), and for BOLD $\Delta\chi$ range (E)

quantitative physiological interpretation of BOLD to help estimate $CMRO_2$; and (2) quantifying CBV or perfusion by modeling the signal from an intravascular contrast agent. An important difference between these 2 applications is that for the BOLD effect the blood susceptibility is altered nonuniformly, weighted by deoxyhemoglobin with the largest changes in the venous vessels, whereas injected contrast agents change the susceptibility of blood uniformly and the concentration of $\Delta\chi$ is usually higher compared with the range relevant for BOLD fMRI. Here we report the behavior of β at different magnetic field strengths and concentrations of $\Delta\chi$ based on numerical simulations using realistic vascular anatomical models derived from detailed imaging in mice.

Results from both VAN modeling using real microvascular networks and Monte-Carlo simulations using randomly orientated infinite cylinders show that proton diffusion effects are less relevant at higher fields for the susceptibility effect, reflected in our finding that β decreases toward a value of 1.0 as the field increases. A value of β greater than 1.0 occurs when there is some degree of motional narrowing due to diffusing protons sampling a range of the distorted fields around a vessel. In the limit of very fast diffusion, so that each proton samples all of the field offsets within the diffusion length, $\beta = 2.0$. Although the extent of proton diffusion is independent of the field strength, the volume of significantly distorted magnetic field around a vessel does increase with the field strength. The observed behavior is implied in the definition of the motional narrowing regime in which diffusion is important (i.e., $\frac{R^2\delta\omega}{D} \ll 1$), as in earlier studies.[5,18] Here, D is the proton diffusion coefficient, $\delta\omega \propto B_0$ is in units of angular frequencies, and R is the radius of cylinders. This relation can be recast as $B_0 R^2 \ll constant$; thus, increasing B_0 requires a smaller $R$for the condition to be satisfied. At higher field strength, the critical vessel radius where β deviates from 1 is smaller, which is consistent with the results shown in Figure 2. The second effect of motional narrowing is that because each proton is sampling a range of field offsets, the net signal decay is reduced compared with what it would have been without diffusion. This is illustrated in Figure 7, showing that the decay is faster around larger vessels and at higher fields, because there is less motional narrowing. Note that both large and small vessels produce faster decay at higher fields, as expected, but the changes in

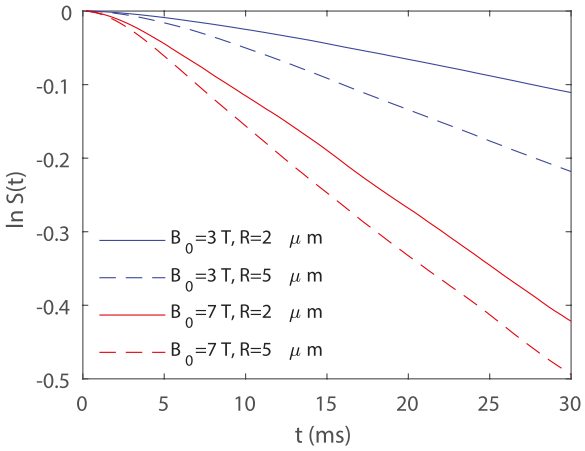

FIGURE 7 Example of ln *S(t)* obtained from Monte-Carlo simulations of random cylinders as in Figure 3A for different B_0 and *R*. Here, $\Delta\chi = 1.2 \times 10^{-6}$ is the same for the 4 curves

the proportions between the larger and smaller vessels are different, reflecting the reduction of motional narrowing at higher fields.

Although the theoretically predicted value of β is between 1 and 2, we see in Figure 2A that there is 1 animal (mouse 4) in which β drops below 1. There are also several $\beta < 1$ values in Figure 5A. This is probably because the voxel size is limited and a single vessel dominates, in which the random network predictions of β varying between 1 for static dephasing and 2 for motional narrowing no longer holds. Recent experiments have also found β to be 0.8 in rodent brain,[34] which could also be related to an ordered, as opposed to random, network structure. This behavior of β may be more prominent for high-resolution fMRI studies in which the dominant effect of single vessels on the MRI signal becomes more likely.

For BOLD fMRI studies, the value of β appears in the Davis model[12,35] and is used to compute $CMRO_2$ changes, but the spatial nonuniformity of $\Delta\chi$ was not fully addressed in the original studies. This complexity makes the measurement of β in the Davis model challenging. The value of β was obtained from fitting the macroscopic Davis model in Ref 23. Treating β as a free-fitting parameter is simple to implement, but it no longer maintains its physiological meaning as the parameter that governs the susceptibility effect, and the 3 parameters M, α, and β are correlated. In VAN modeling, we are able to compute the oxygen distribution within microvascular networks, which provides the microscopic distributions of deoxyhemoglobin concentrations. This enables us to compute the physiological parameter β that is relevant for the Davis model from first principles. Compared with the uniform $\Delta\chi$ results, deoxyhemoglobin-weighted results show that β is closer to the large vessel limit, as the vessels that contain the most deoxyhemoglobin are large venules. As shown in Figure 2B, $\beta \approx 1.1$ for $B_0 = 1.5$T, and $\beta = 1$ at $B_0 = 3$T and above, as opposed to the early calculations of $\beta = 1.5$ at 1.5 T[12] and $\beta = 1.3$ at 3 T.[36]

The study of the field strength dependence on the susceptibility effect provides guidance for CBV measurements in imaging based on contrast agents. One assumption for these techniques is that $\Delta R_2^* \propto \text{CBV}$, and thus the map of an R_2^* increase after injection of a contrast agent provides a map of CBV.[1-4] However, a hidden assumption here is that β is uniform, as $\Delta R_2^* \propto \text{CBV} * (\Delta\chi)^\beta$, and this relation is not accurate if β varies within regions. To obtain a more accurate measurement of CBV, a map of β or a sense of how β changes within different regions is desired to correct estimates of CBV. We have shown in Figure 5A that for a uniform distribution of $\Delta\chi$ within the contrast agent range, $\beta \approx 1$ except at $B_0 = 14$T. This indicates that a lower concentration of $\Delta\chi$ is desired for $B_0 = 14$T, as shown in Figure 5B.

5 | CONCLUSIONS

We have analyzed the susceptibility effect on the transverse relaxation rate using realistic microvascular anatomical networks and modeling of the oxygen advection and diffusion through the network. Both the uniform and the deoxyhemoglobin-weighted distribution of $\Delta\chi$ were studied. We show that the parameter β, which governs the dependence of the transverse relaxation rate on the magnetic susceptibility shift, is closer to the large vessel limit of $\beta = 1$ at higher magnetic field strength. For BOLD fMRI, with a realistic anatomy and distribution of hemoglobin saturation, our results indicate that $\beta = 1$ for 3 T and above, greatly simplifying macroscopic models such as the Davis model.[12] For perfusion and functional imaging techniques based on contrast agents, $\beta = 1$ for 9.4 T and below, in general. Our work provides insights on the fundamental question of the effect of proton diffusion on MR signals at different field strengths as well as practical applications for CBV measurements with contrast agents and $rCMRO_2$ measurements with BOLD fMRI.

ACKNOWLEDGMENTS

This work is supported by the NIH NIBIB (grants P41-EB015896 and R01-EB019437), the NIH NINDS (grant R01-NS036722), the BRAIN Initiative (NIH NIMH grants R01-MH111419 and R01-MH111359), and the MGH/HST Athinoula A. Martinos Center for Biomedical Imaging.

REFERENCES

1. Mandeville JB, Jenkins BG, Chen Y-CI, et al. Exogenous contrast agent improves sensitivity of gradient-echo functional magnetic resonance imaging. *Magn Reson Med*. 2004;52:1272–1281.

2. Qiu D, Zaharchuk G, Christen T, Ni WW, Moseley ME. Contrast-enhanced functional blood volume imaging (CE-fBVI): enhanced sensitivity for brain activation in humans using the ultrasmall superparamagnetic iron oxide agent ferumoxytol. *NeuroImage*. 2012;62:1726–1731.
3. Rosen BR, Belliveau JW, Vevea JM, Brady TJ. Perfusion imaging with NMR contrast agents. *Magn Reson Med*. 1990;14:249–265.
4. Weinstein JS, Varallyay CG, Dosa E, et al. Superparamagnetic iron oxide nanoparticles: diagnostic magnetic resonance imaging and potential therapeutic applications in neurooncology and central nervous system inflammatory pathologies, a review. *J Cereb Blood Flow Metab*. 2010;30:15–35.
5. Boxerman JL, Hamberg LM, Rosen BR, Weisskoff RM. MR contrast due to intravascular magnetic susceptibility perturbations. *Magn Reson Med*. 1995;34:555–566.
6. Ogawa S, Lee TM, Kay AR, Tank DW. Brain magnetic resonance imaging with contrast dependent on blood oxygenation. *Proc Natl Acad Sci*. 1990;87:9868–9872.
7. Thulborn KR, Waterton JC, Matthews PM, Radda GK. Oxygenation dependence of the transverse relaxation time of water protons in whole blood at high field. *Biochim Biophys Acta*. 1982;714:265–270.
8. Kwong KK, Belliveau JW, Chesler DA, et al. Dynamic magnetic resonance imaging of human brain activity during primary sensory stimulation. *Proc Natl Acad Sci*. 1992;89:5675–5679.
9. Lin A-L, Fox PT, Yang Y, Lu H, Tan L-H, Gao J-H. Evaluation of MRI models in the measurement of CMRO2 and its relationship with CBF. *Magn Reson Med*. 2008;60:380–389.
10. Logothetis NK, Pauls J, Augath M, Trinath T, Oeltermann A. Neurophysiological investigation of the basis of the fMRI signal. *Nature*. 2001;412:150–157.
11. Ogawa S, Menon RS, Tank DW, et al. Functional brain mapping by blood oxygenation level-dependent contrast magnetic resonance imaging. A comparison of signal characteristics with a biophysical model. *Biophys J*. 1993;64:803–812.
12. Davis TL, Kwong KK, Weisskoff RM, Rosen BR. Calibrated functional MRI: mapping the dynamics of oxidative metabolism. *Proc Natl Acad Sci*. 1998;95:1834–1839.
13. Gauthier CJ, Hoge RD. A generalized procedure for calibrated MRI incorporating hyperoxia and hypercapnia. *Hum Brain Mapp*. 2013;34:1053–1069.
14. Grubb RL, Raichle ME, Eichling JO, Ter-Pogossian MM. The effects of changes in PaCO2 on cerebral blood volume, blood flow, and vascular mean transit time. *Stroke*. 1974;5:630–639.
15. Mandeville JB, Marota JJ, Ayata C, et al. Evidence of a cerebrovascular postarteriole windkessel with delayed compliance. *J Cereb Blood Flow Metab*. 1999;19:679–689.
16. Hoge RD. Calibrated fMRI. *NeuroImage*. 2012;62:930–937.
17. Pike GB. Quantitative functional MRI: concepts, issues and future challenges. *NeuroImage*. 2012;62:1234–1240.
18. Kiselev VG, Posse S. Analytical theory of susceptibility induced NMR signal dephasing in a cerebrovascular network. *Phys Rev Lett*. 1998;81:5696.
19. Yablonskiy DA, Haacke EM. Theory of NMR signal behavior in magnetically inhomogeneous tissues: the static dephasing regime. *Magn Reson Med*. 1994;32:749–763.
20. Stables LA, Kennan RP, Gore JC. Asymmetric spin-echo imaging of magnetically inhomogeneous systems: theory, experiment, and numerical studies. *Magn Reson Med*. 1998;40:432–442.
21. Croal PL, Driver ID, Francis ST, Gowland PA. Field strength dependence of grey matter R2* on venous oxygenation. *NeuroImage*. 2017;146:327–332.
22. Griffeth VE, Buxton RB. A theoretical framework for estimating cerebral oxygen metabolism changes using the calibrated-BOLD method: modeling the effects of blood volume distribution, hematocrit, oxygen extraction fraction, and tissue signal properties on the BOLD signal. *NeuroImage*. 2011;58:198–212.
23. Gagnon L, Sakadžić S, Lesage F, et al. Validation and optimization of hypercapnic-calibrated fMRI from oxygen-sensitive two-photon microscopy. *Phil Trans R Soc B*. 2016;371:20150359.
24. Gagnon L, Sakadžić S, Lesage F, et al. Quantifying the microvascular origin of BOLD-fMRI from first principles with two-photon microscopy and an oxygen-sensitive nanoprobe. *J Neurosci*. 2015;35:3663–3675.
25. Fang Q, Sakadžić S, Ruvinskaya L, Devor A, Dale AM, Boas DA. Oxygen advection and diffusion in a three dimensional vascular anatomical network. *Opt Express*. 2008;16:17530.
26. Fang Q, Boas DA. Tetrahedral mesh generation from volumetric binary and grayscale images. In: Proceedings of the 2009 IEEE International Symposium on Biomedical Imaging: From Nano to Macro, Boston, MA; 2009: 1142–1145.
27. Pathak AP, Ward BD, Schmainda KM. A novel technique for modeling susceptibility-based contrast mechanisms for arbitrary microvascular geometries: the finite perturber method. *NeuroImage*. 2008;40:1130–1143.
28. Uludağ K, Müller-Bierl B, Uğurbil K. An integrative model for neuronal activity-induced signal changes for gradient and spin echo functional imaging. *NeuroImage*. 2009;48:150–165.
29. Martindale J, Kennerley AJ, Johnston D, Zheng Y, Mayhew JE. Theory and generalization of Monte Carlo models of the BOLD signal source. *Magn Reson Med*. 2008;59:607–618.
30. Spees WM, Yablonskiy DA, Oswood MC, Ackerman JJ. Water proton MR properties of human blood at 1.5 Tesla: magnetic susceptibility, T(1), T(2), T*(2), and non-Lorentzian signal behavior. *Magn Reson Med*. 2001;45:533–542.
31. Chu K-. C, Xu Y, Balschi JA, Springer CS. Bulk magnetic susceptibility shifts in NMR studies of compartmentalized samples: use of paramagnetic reagents. *Magn Reson Med*. 1990;13:239–262.
32. Báez-Yánez MG, Ehses P, Mirkes C, Tsai PS, Kleinfeld D, Scheffler K. The impact of vessel size, orientation and intravascular contribution on the neurovascular fingerprint of BOLD bSSFP fMRI. *NeuroImage*. 2017;163:13–23.
33. Parker GJM, Roberts C, Macdonald A, et al. Experimentally-derived functional form for a population-averaged high-temporal-resolution arterial input function for dynamic contrast-enhanced MRI. *Magn Reson Med*. 2006;56:993–1000.
34. Shu CY, Sanganahalli BG, Coman D, Herman P, Rothman DL, Hyder F. Quantitative β mapping for calibrated fMRI. *NeuroImage*. 2016;126:219–228.
35. Hoge RD, Atkinson J, Gill B, Crelier GR, Marrett S, Pike GB. Investigation of BOLD signal dependence on cerebral blood flow and oxygen consumption: the deoxyhemoglobin dilution model. *Magn Reson Med*. 1999;42:849–863.
36. Bulte DP, Drescher K, Jezzard P. Comparison of hypercapnia-based calibration techniques for measurement of cerebral oxygen metabolism with MRI. *Magn Reson Med*. 2009;61:391–398.

SUPPORTING INFORMATION

Additional supporting information may be found online in the Supporting Information section at the end of the article.

FIGURE S1 A, Distribution of vessel sizes from the 6 networks of mouse vasculature measured in vivo. B, Value of β obtained from the random cylinder model with the vessel size distribution in (A) for both BOLD ($\mathbf{2\times10^{-7}}$ to $\mathbf{12\times10^{-7}}$) and contrast agent range ($\mathbf{1\times10^{-6}}$ to $\mathbf{10\times10^{-6}}$) of $\boldsymbol{\Delta\chi}$ concentration. C, Value of β as a function of $\boldsymbol{\Delta\chi}$ concentration in SI units

FIGURE S2 A, Vasculature (blue, veins; red, arteries; green, capillaries) with starting pial artery and vein (branching order = 0) indicated in the figure. B, Distribution of $\boldsymbol{SO_2}$ computed in the model as a function of branching orders, starting from the pial artery and vein. C, $\boldsymbol{\Delta\chi}$ concentration in different branching orders. D, Corresponding vessel diameter in different branching orders

FIGURE S3 Value of β obtained for a mouse vascular for different dt values in the Monte-Carlo simulations for the BOLD range of $\boldsymbol{\Delta\chi}$ ($\mathbf{2\times10^{-7}}$ to $\mathbf{12\times10^{-7}}$) (A) and contrast agent range of $\boldsymbol{\Delta x}$ ($\mathbf{1\times10^{-6}}$ to $\mathbf{10\times10^{-6}}$) (B)

How to cite this article: Cheng X, Berman AJL, Polimeni JR, et al. Dependence of the MR signal on the magnetic susceptibility of blood studied with models based on real microvascular networks. *Magn Reson Med.* 2019;00:1–10. https://doi.org/10.1002/mrm.27660